Available online at website: https://journal.bcrec.id/index.php/bcrec

Bulletin of Chemical Reaction Engineering & Catalysis, 19 (4) 2024, 649-657

Research Article

Photoreduction of CO_2 to Formic Acid in Aquatic Phase Using Layer Double Hydroxide (LDH) Catalyst

Jenny Rizkiana[1,2,3*], Dzaky Auliardi[1], Aghietyas Choirun Az Zahra[2,3], Francesco Thadeo[1], Wibawa Hendra Saputera[1], Tatang Hernas Soerawidjaja[1,2], Hary Devianto[1]

[1]Department of Chemical Engineering, Faculty of Industrial Technology, Institut Teknologi Bandung, Jalan Ganesha 10 Bandung, 40132, Indonesia
[2]Department of Bioenergy Engineering and Chemurgy, Faculty of Industrial Technology, Institut Teknologi Bandung, Jl. Let. Jend. Purn. Dr. (HC) Mashudi No.1, Sumedang, 45363, Indonesia
[3]Center for Catalysis and Reaction Engineering, Institut Teknologi Bandung, Jalan Ganesha 10 Bandung, 40132, Indonesia

Received: 18th August 2024; Revised: 1st December 2024; Accepted: 2nd December 2024
Available online: 3rd December 2024; Published regularly: December 2024

Abstract

The increasing accumulation of CO_2, the primary greenhouse gas (GHG), in the Earth's atmosphere has caused significant environmental problems and adverse climate change. Photoreduction offers promising method to convert CO_2 into high value chemical compounds, such as formic acid, which can serve as a hydrogen carrier. The process of photoreduction efficiency can be enhanced by using photocatalyst capable of operating across two distinct photosystems each having a different spectrum based on the sensitivity of light. This study aims to investigate the impact of the photocatalyst preparation conditions on the activity of the resulting photocatalyst and identify which is the most effective one on the formic acid production. Photocatalysts based on Layered Double Hydroxide (LDH) composed of zinc and chromium was synthesized, resulting in Zn-Cr LDH, which was subsequently enhanced by incorporating Cu and Cu_2O. The operating temperature varied at 60 ℃ and 100 ℃. The highest yield of formic acid of 21,62 $\mu mol.g_{cat}^{-1}.hr^{-1}$ was obtained at a reaction temperature of 100 ℃ using 0.3Cu@Zn-Cr LDH. This photocatalyst shows increased activity when the reaction temperature is increased to 60 ℃ and 100 ℃. In contrast, 0.3Cu_2O@Zn-CrLDH showed a decreased activity at the elevated temperatures. This discrepancy attributed to the self-oxidation mechanism of Cu and Cu_2O; while the oxidation of 0.3Cu@Zn-CrLDH results in Cu_2O which retains photocatalytic activity, the oxidation of 0.3Cu_2O@Zn-CrLDH leads to inactive CuO. This study provides valuable insight into the material design and demonstrates the potential of Cu-modified Zn-Cr LDH for sustainable CO_2 reduction applications.

Keywords: Photocatalyst; Photoreduction; Formic Acid; Carbon Dioxide; Layer Double Hydroxide

How to Cite: Rizkiana, J., Auliardi, D., Az Zahra, A.C., Thadeo, F., Saputera, W.H., Soerawidjaja, T.H., Devianto, H. (2024). Photoreduction of CO_2 to Formic Acid in Aquatic Phase Using Layer Double Hydroxide (LDH) Catalyst. *Bulletin of Chemical Reaction Engineering & Catalysis*, 19 (4), 649-657 (doi: 10.9767/bcrec.20199)

Permalink/DOI: https://doi.org/10.9767/bcrec.20199

1. Introduction

Since the mid-20th century, rapid industrial development has led to serious environmental pollution and the exploitation of natural resources. The increased use of high-energy-density fossil fuels has resulted in a surge in CO_2 emissions, causing environmental problems. The excessive accumulation of greenhouse gases (GHG), particularly CO_2, has led to climate change with serious consequences for environmental sustainability and human comfort. In 2019, the World Meteorological Organization (WMO) reported that atmospheric CO_2 levels had reached 407.8 parts per million (ppm), far above the pre-industrial level of around 270 ppm. Comprehensive research stated that the safe level of CO_2 levels should be below 350 ppm [1].

Several techniques have been explored for CO_2 reduction and utilization, including electro- /

* Corresponding Author.
Email: rizkiana@itb.ac.id (J. Rizkiana)

photo- / photo-electro-chemical and thermochemical conversion, and biological fixation [2]. Electrochemical techniques for converting CO_2 into higher value chemicals using electrical energy are still relatively ineffective, partly due to the electrode stability issues [3]. Likewise, the biological transformation of CO_2 into useful products by microalgae still has various limitations [4]. The thermal and catalytic conversion of CO_2 to methane (CH_4) and carbon monoxide (CO) using transitional metal catalysts requires high temperatures and pressures due to the nature of highly endothermic reactions which increased the operational cost [5].

Photocatalytic techniques, which mimics photosynthesis, are thus termed artificial photosynthesis, offer a promising route. These techniques utilize solar energy and water, both abundant and freely available resources, to reduce CO_2 to formic acid (HCOOH), formaldehyde (HCHO), methanol (CH_3OH), or methane (CH_4). The photo-reduction of CO_2 to formic acid is particularly interesting due to its potential to reduce the amount of CO_2 levels in waste or exhaust gas and in the free atmosphere, while producing formic acid [6]. Formic acid is non-toxic, biodegradable, and has a good energy density [7]. It can also serve as a base compound for producing other chemicals as it contains active carbonyl and hydroxyl groups, allowing esterification, dehydration, and formylation reactions to take place [8]. Additionally, formic acid has been identified as a hydrogen carrier with a large hydrogen storage capacity of 53gram H_2/L [9]. Using formic acid as a hydrogen carrier shifts the hydrogen raw material supply from natural gas has to CO_2 from industrial exhaust gases.

Despite its potential, CO_2 photoreduction research faces various challenges. It requires a light-sensitive semiconductor-based catalyst in aqueous solution [10,11]. Previous studies have explored CO_2 reduction to formic acid using a $Zn_2Ti_{2.5}A_{0.5}O_{7.75}$ catalyst under atmospheric pressure, room temperature, and using three LED light sources. The basic principle of photoreduction is to replicate the photosynthetic reaction in plants using metal oxide catalysts. The process begins with the formation of holes and electrons resulting photon energy absorption, which then react with CO_2 on the surface of the catalyst following the reaction of:

$$CO_2 + 2H^+ + 2e^- \rightarrow HCOOH \quad (1)$$

However, not all electrons react with CO_2 due to its inertness and stability of CO_2.

Photoreduction offers excellent opportunities, but the low CO_2 conversion remains the biggest obstacle. Some factors causing this issue are low solubility of CO_2 in water, the competition between water and CO_2 for reduction, and photocatalyst performance. Various materials have been studied as CO_2 scavengers and photocatalysts, such as organic sorbents, zeolite, activated carbon, titania nanotubes, TiO_2, Bi_2WO_6 and layered double hydroxides (LDH) [12]. Among these, LDH has received considerable attention as a high-temperature (200-500 ℃) CO_2 sorbent due to its high CO_2 adsorption capacity in layered space and its semiconductor properties [13]. LDH-based materials have a large specific surface area and high affinity for CO_2 molecules facilitating the selective conversion of CO_2 under the light. The intrinsic properties of LDH have made it a promising material for CO_2 adsorption and photoreduction applications [13]. Zn-Cr LDH has been shown to successfully catalyze the water splitting reaction under visible light irradiation [14]. Bolton demonstrated that fuel-generation reactions using photon energy for energy storage are most efficient when two photosystems operate in series in an oxidation-reduction reaction [15]. Formic acid formation requires light wavelengths below 543 nm for one photosystem and below 804 nm for two photosystems. Zn-Cr has the maximum light absorbance at 570-590 nm. Thus, an additional photosystem is needed to complement the light absorption by Zn-Cr LDH. One way to mitigate is by introducing materials such as Cu and Cu_2O which have a broader light absorption at 300-634 nm range [16].

This study aims to improve the catalytic performance of Zn-Cr LDH for visible light-driven CO_2 reduction by introducing Cu and Cu_2O as complementary components. The effect of modifying Zn-Cr LDH with Cu and Cu_2O on the photocatalyst's structural properties, light absorption, and photocatalytic activity is investigated. The coprecipitation pH during Zn-Cr LDH preparation is observed to see the impact on the structural and phase properties, particularly the formation of zincite phase. Reaction condition such as temperature are also optimized to maximize the formic acid yield. The mechanistic role of Cu and Cu_2O in the photocatalytic process is being examined. Through this study, it is expected to provide valuable insights into material design and illustrate the potential of Cu-modified Zn-Cr LDH for sustainable CO_2 reduction applications.

2. Materials and Methods

2.1 Instruments and Materials

The materials used for the preparation of the photocatalyst are NaOH, Na_2CO_3, $Zn(NO_3)_2.4H_2O$, $Cr(NO_3)_3.9H_2O$, HN_3, $Cu(COOH)_2$, distilled water, and N_2 gas. The materials used in the main experiment are CO_2 gas, distilled water and pyridine. Pyridine was added to the solution as an electron donor ligand to enhance formic acid recovery. It reduces the bond energy of formate on photocatalyst surface thereby increasing the hydrogenation activity by

increasing the desorption of formate, the rate-limiting step [17] The equipment for preparing the photocatalyst included a burette, statives and clamps, measuring flasks, and Buchner funnels. The main equipment used in the photoreduction process is an Erlenmeyer flask, 35 cm × 37 cm × 35 cm irradiation box, magnetic stirrer, heater, 300 W LED lamp, and sparger. The main instrumental scheme is shown in Figure 1.

2.2. Photocatalyst Preparation

The first solution was the mixture of NaOH 2 M and Na_2CO_3 0.125 M which then was transferred to the first burette. Inside the second burette was $Zn(NO_3)_2.4H_2O$ 0.75 M and $Cr(NO_3)_3.9H_2O$ 0.25 M. A solution with a pH of 4.0 – 4.5, adjusted with nitric acid (HNO_3) or left neutral, was prepared and transferred to a coprecipitation flask. Both solutions were then added dropwise at a controlled rate to the flask, while maintaining the pH within the specified range of 4-4.5 or 8-9 by adding nitric acid or dilute NaOH. This pH allows the precipitation of Zn and Cr [18,19]. The resulting precipitate was filtered, washed thoroughly until it reached the normal pH. The solid obtained, $Zn_6Cr_2(OH)_{16}(CO_3).4H_2O$, was then dried to a constant weight before being stored in a clean, dry container.

The synthesis of Cu_2O@Zn-Cr LDH was performed using an ion-exchange method which can be denoted as'$3xCu_2O@Zn_{6-6x}Cr_2(OH)_{16}(CO_3).4H_2O$' (x = 30%). Where the value of x represents the percentage of Cu_2O that substitutes Zn atoms on the surface of $Zn_6Cr_2(OH)_{16}(CO_3).4H_2O$. The process begins with the introduction of Cu_2O to the pre-synthesized Zn-Cr LDH. The mixture was stirred, filtered, and washed to remove excess Cu^{2+} ions, followed by treatment with formic acid. The solid, $Cu_{6x}Zn_{6-6x}Cr_2(OH)_{16}(CO_3).4H_2O$' (x = 30%), was then heated at 130 °C or 200 °C under a nitrogen atmosphere, filtered, washed again, and dried to a constant weight. The final powder was stored in a clean, dry, and labeled container.

2.3. Main Experiment

The photoreduction reaction was conducted in an Erlenmeyer flask, illuminated by a 300-W LED spotlight in a box measuring 35 cm × 37 cm × 35 cm equipped with mirrors on each plane, referred to as a photoreactor set. Each reaction began with the saturation of CO_2 into a solution containing 0.3 M pyridine by continuously flowing CO_2 gas into the photoreactor system for 4 hours without irradiation. Upon the completion of the saturation, photocatalyst was added to the Erlenmeyer flask, the 300-W LED spotlight was turned on, and CO_2 gas was continuously flowed for 8 hours. Each experiment utilized 400 mg of photocatalyst in 200 mL of solution. The CO_2 gas feed which derived from fermented sugar, produced a CO_2 gas flow rate of 12 mL/min (25 °C, 1 atm). During both saturation and reaction phase, the solution was stirred using a magnetic stirrer. The pH of the reaction solution was monitored as an early detection of formic acid presence in the solution.

Each photocatalyst sample was characterized using X-Ray Diffraction (XRD) and UV-Vis diffuse reflectance spectroscopy. The final product was analyzed using Gas Chromatography Mass Spectrometry (GC-MS, Agilent, J&W Scientific, HP-5MS capillary column), with helium as the carrier gas.

3. Results and Discussion

3.1 Photocatalyst Characteristic Result

The photocatalysts prepared and characterized in this study are: $Zn_6Cr_2(OH)_{16}(CO_3).4H_2O$ which is made at coprecipitation pH = 8, then referred to as Zn-CrLDH8; $Zn_6Cr_2(OH)_{16}(CO_3).4H_2O$ which is made at coprecipitation pH = 4, then referred to as Zn-CrLDH4; $0.9Cu_2O@Zn_4.2Cr_2(OH)_{16}(CO_3).4H_2O$ made by the ion exchange method, where Cu_2O substitutes 30%-Zn in $Zn_6Cr_2(OH)_{16}(CO_3).4H_2O$, then denoted as $0.3Cu_2O$@Zn-CrLDH; $1.8Cu_2O@Zn_4.2Cr_2(OH)_{16}(CO_3).4H_2O$ prepared by the ion exchange method, where Cu substitutes 30%-Zn in $Zn_6Cr_2(OH)_{16}(CO_3).4H_2O$, then denoted as 0.3Cu@Zn-CrLDH.

In this research, the characterization of photocatalysts was carried out using X-Ray Diffraction (XRD) and UV-Vis diffuse reflectance spectroscopy. The diffractogram from the XRD test results was processed using the Match application version 3.0 and Crystallography Open Database (COD) to confirm the formed phases. Interpretation of XRD data can determine the distance between planes in the sample and the crystallinity of the photocatalyst using the Bragg equation. The reflectance data from the UV-Vis DRS test was processed and interpreted using the Kubelka-Munk (F(R)) equation.

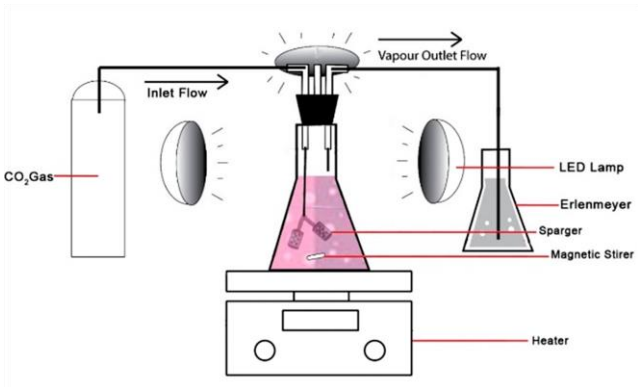

Figure 1. Main instrumental scheme.

3.1.1 Photocatalyst crystalography characteristic

The diffractogram patterns for Zn-CrLDH8, Zn-CrLDH4, 0.3Cu_2O@Zn-CrLDH and 0.3Cu@Zn-CrLDH are presented in Figure 2. In this figure, the diffractogram for Zn-CrLDH8 exhibited sharper peaks at the Miller *hkl* index (003) and (006) compared to Zn-CrLDH4. Zn-CrLDH8 has a lattice plane (003) with a *d*-spacing of 7.63 Å, resulting in a basal spacing of 3*d*003=22.89 Å along the c-axis. The diffractogram pattern was confirmed by the Crystallography Open Database (COD) to resemble that of natural stichtite ($Mg_6Cr_2(OH)_{16}CO_3.4H_2O$), an isostructure of hydrotalcite ($Mg_6Al_2(OH)_{16}CO_3.4H_2O$) which typically exhibits a lattice plane (003) at 7.76 Å [18]. Thus, the lattice parameters for the Zn-CrLDH8 were determined to be a = 3.02 Å and c = 22.89 Å. In addition, Zn-CrLDH8 exhibited a purplish-pink color, closely resembling the natural color of stichtite [18]. As seen in Figure 2, the Zn-CrLDH8 sample displayed additional crystalline phase beyond stichtite. According to Kloprogge [19], the secondary phase observed at pH of 7-12 corresponds to zincite (ZnO), and a decrease in the pH results in reduction of the zincite peak intensity.

The diffractogram for the Zn-CrLDH4 sample showed subtle differences compared to Zn-CrLDH8, with the lattice (003) peak appearing at the same *d*-spacing of 7.76 Å [18]. The lattice parameters for the Zn-CrLDH4 were a = 3.01 Å and c = 23.28 Å, indicating a larger three-layered rhombohedral cell (c-axis). Kloprogge proposed several explanations for this observation, including (i) the incorporation of more interlayer species in the interlayer region, or (ii) changes in the sequence of interlayer and brucite-like layer species, or (iii) the acidic pH of the synthesis process might lead to on intercalations of chromium(III) complexes (e.g. $[Cr(OH)x]^{3-x}$) or chromium(VI) (CrO_4^{2-}) complexes [19]. It was also suspected that low pH may reduce Cr^{3+} incorporation into the brucite layer, leading to fewer positive charges within the layers, leading to a larger interlayer spacing in the c-axis distance [19]. The Zn-CrLDH4 sample showed no secondary phase and exhibited higher crystallinity (61.0%) compared to Zn-CrLDH8 sample (46.8%). In addition, the Zn-CrLDH4 displayed a darker purple color, indicating the presence of different coordination complexes.

Samples of 0.3Cu@Zn-CrLDH and 0.3Cu_2O@Zn-CrLDH were prepared via ion exchange, where some Zn^{2+} atoms in Zn-CrLDH8 were substituted with Cu^{2+} atoms, followed by reduction with formic acid to form Cu^+. Upon thermal treatment, Cu^+ transformed into Cu_2O(s) at 130 °C and to Cu(s) at 200 °C. Zn-CrLDH8 was chosen based on its better photocatalytic performance compared to Zn-CrLDH4 (discussed further in Section 3.2.1). As shown in Figure 2, the 0.3Cu@Zn-CrLDH exhibited Cu(s) peak in the lattice plane (111) with a *d*-spacing of 2.088 Å. The lattice parameter for Cu (s) phase was determined to be 3.617 Å, consistent with the values reported by Clark *et al.* [20].

Figure 3 presents a more detailed diffractogram pattern between 2θ values of 35°-55° to compare the 0.3Cu_2O@Zn-CrLDH and the Zn-CrLDH8. The 0.3Cu_2O@Zn-CrLDH found to have a diffraction peak corresponding to the (111) and (020) planes of the cuprite (Cu_2O). The lattice parameter for this sample was 4.258 Å, in agreement with values reported by Neuburger (1930) [21]. An important observation was the shift of (003), (006), (012), and (110) peaks for both 0.3Cu@Zn-CrLDH and 0.3Cu_2O@Zn-CrLDH towards a larger 2θ, indicating a decrease of d-spacing and lattice parameters. This indicates a

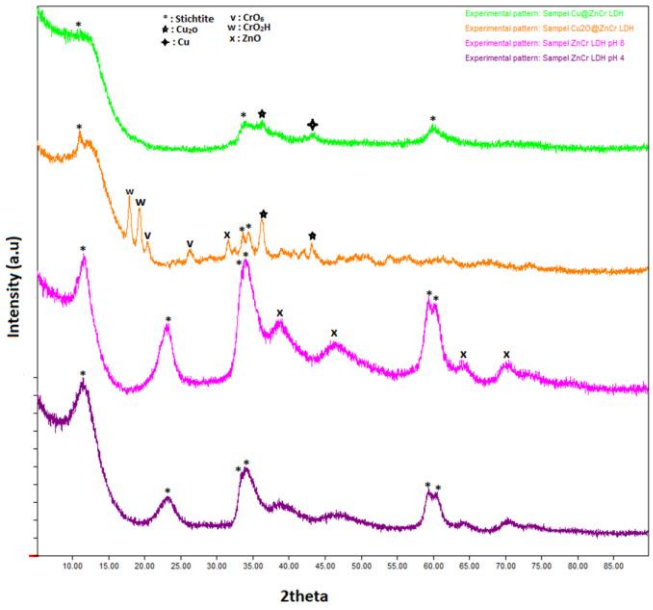

Figure 2. Diffractogram pattern of each sample from the bottom up: Zn-CrLDH8, Zn-CrLDH4, 0.3Cu_2O@Zn-CrLDH and 0.3Cu@Zn-CrLDH

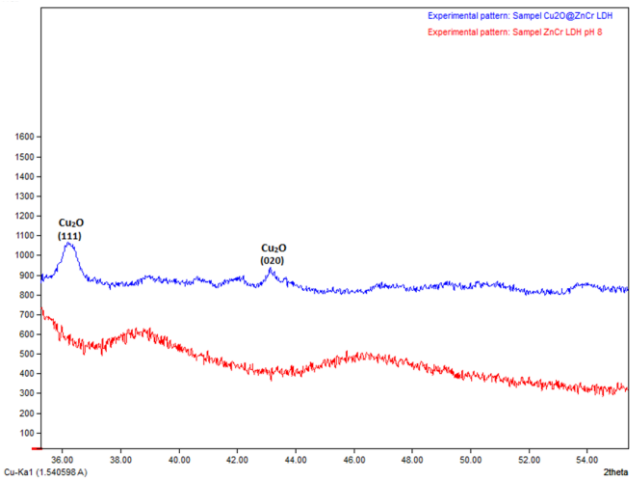

Figure 3. Comparison of the 0.3Cu_2O@Zn-CrLDH sample and the Zn-CrLDH8 at 2θ 35°-55°

shrinkage of the three-layered rhombohedral unit cell, likely due to the incorporation or substitution of Cu^{2+} into Zn-CrLDH. The smaller ionic radius of the Cu^{2+} ion (1 pm smaller than that of Zn^{2+}) and the Jahn-Teller effect in octahedral $Cu(OH)_6$ complexes likely result in shorter the Cu–O bonds in the xy-plane, contributing to a decrease in the cation-cation spacing [22].

In the $0.3Cu_2O$@Zn-CrLDH sample, additional phases such as CrO_3, ZnO, and CrO_2H were identified through the Match application (v 3.0) and Crystallography Open Database (COD). In addition, both the $0.3Cu_2O$@Zn-CrLDH and 0.3Cu@Zn-CrLDH were amorphous, as indicated by a reduction in in crystallinity and a change in the hydrotalcite structure of Zn-CrLDH. The decrease in crystallinity and structural alterations may be attributed to the interaction of formic acid with the LDH structure. However, the precise amount of formic acid required to reduce Cu^{2+} to Cu^{+} and Cu^{0} was not quantified in this study.

3.1.2 Photocatalyst spectroscopy characteristic

Figure 4 presents the UV-Vis diffuse reflectance spectra for samples of Zn-CrLDH8, Zn-CrLDH4, $0.3Cu_2O$@Zn-CrLDH and 0.3Cu@Zn-CrLDH. The recorded spectra was converted into the Kubelka-Munk function (F(R)) from the reflectance data. In the ultraviolet region, all samples showed an intrinsic absorption band attributed to metal-to-ligand charge transfer (LMCT) from the O-2p orbital to the Zn-4s and Cr-3d-e_g orbitals [19]. The absorption band between 345-485 nm is associated with metal–metal charge transfer (MMCT) from Cr-3d-t_{2g} to Zn-4s [22]. In the visible region, two prominent peaks at 580 nm and 655 nm are indicative of *d-d* transitions in Cr^{2+} ions, specifically the

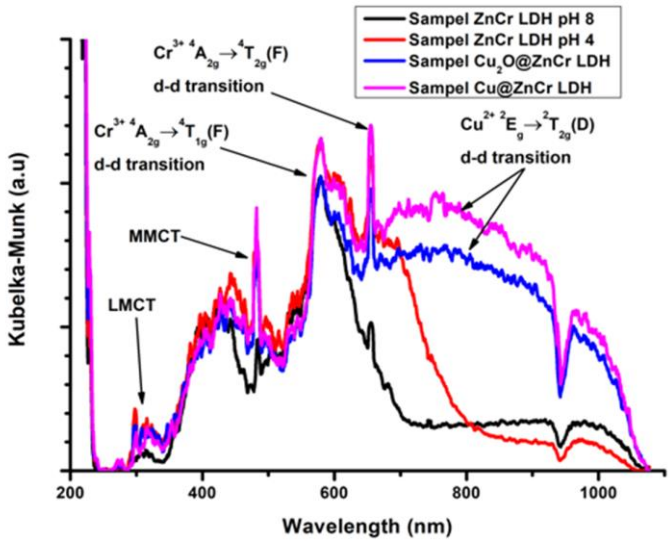

Figure 4. UV-Vis diffuse reflectance spectroscopy for samples of Zn-CrLDH8, Zn-CrLDH4, $0.3Cu_2O$@Zn-CrLDH and 0.3Cu@Zn-Cr LDH

$^4A_{2G} \rightarrow {}^4T_{1G}$ (F) and $^4A_{2G} \rightarrow {}^4T_{2G}$ (F) transitions [23]. In the absorption area of more than 675 nm, the influence of the d-d transition in Cu^{2+} ions ($^2E_g \rightarrow {}^2T_{2g}$ (D)) was seen in the $0.3Cu_2O$@Zn-CrLDH and 0.3Cu@Zn-CrLDH [22]. Consequently, the $0.3Cu_2O$@Zn-CrLDH and 0.3Cu@Zn-CrLDH are expected to perform more effectively than the Zn-CrLDH8 and Zn-CrLDH4 under visible light irradiation.

3.2 Performance of Photocatalysts in the Process of Photreduction of CO_2 to Formic Acid

Figure 5 illustrates the pH of the photoreduced solution after 8 hours of visible light irradiation. Notations 1, 2, 3, and 4 on the abscissa corresponds to the Zn-CrLDH8, Zn-CrLDH4, $0.3Cu_2O$@Zn-CrLDH and 0.3Cu@Zn-CrLDH, respectively. The horizontal line at y=6.85 represents the pH of a saturated solution of CO_2 in a 0.3 M pyridine. A solution with pH below the saturated CO_2 pH indicates the presence of formic acid, as the acid ionization constant (Ka) of formic acid (1.8×10^{-4}) is higher than that of carboxylic acids as CO_2 (4.47×10^{-7}).

3.2.1 Effect of co-precipitation pH in LDH production on photocatalyst performance

The effect of creating a layered double hydroxide (LDH) on photocatalyst performance in the process of photoreduction of CO_2 to formic acid was observed by varying the co-precipitation pH of 4 and 8. As previously outlined, variations in co-precipitation pH affected the crystal structure but did not affect the optical properties of the Zn-CrLDH. As seen in Figure 5, the pH of the photoreduced solution using Zn-CrLDH8 and Zn-CrLDH4 at room temperature remained above the saturated pH of CO_2. This indicates that Zn-Cr LDH has limited photocatalytic activity for CO_2 reduction to formic acid at room temperature, although Zn-CrLDH4 appears to be more effective than Zn-CrLDH8. Increasing the reaction

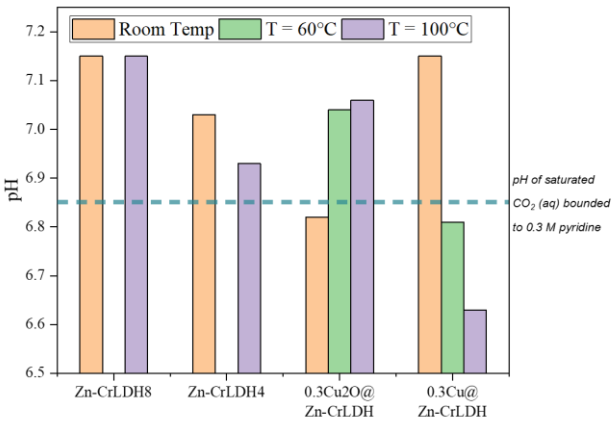

Figure 5. pH of the photoreduction reaction solution for 8 hours under visible light irradiation

temperature to 100 °C was expected to accelerate the reaction; however, this still did not shift the reaction toward formic acid formation, as seen from the pH of the solution remaining above the saturated pH of CO_2 for both Zn-CrLDH8 and Zn-CrLDH4.

The process of CO_2 reduction to formic acid requires a two-electron cycle, similar to the reduction of CO_2 to CO. Jiang *et al.* reported that Zn-Cr LDH also has a limited activity in the photoreduction reaction of CO_2 to CO [19]. After 24-hour reaction time, approximately only 0.1 µmol of CO gas was produced with a small amount of H_2 observed in pure water [21]. However, Zn-CrLDH successful in catalyzing water splitting reactions under visible light irradiation. Parida and Mohapatra proposed a possible mechanism for water splitting using Zn-Cr LDH. Upon exposure to visible light, electrons are excited from O2p to Cr-3d-t_{2g} (LMCT) followed by Cr-3d-t_{2g} to Cr-3deg (d-d transition) in the CrO_6 octahedron [14]. The photoexcited electrons on CrO_6 band, specifically the Cr-3dt_{2g} band, are located just below the H^+/H_2 reduction energy level (-0.41 V vs SHE), while the valence band level of O-2p is more positive than the oxidation energy level of O_2/H_2O (+1.23 V vs SHE), as shown in Figure 6. As a result, water molecules are oxidized by holes in the valence band to form oxygen gas and reduced by electrons in the conduction band to form hydrogen gas. The reduction of H^+ to H_2 causes the increase of pH of the solution, which explains why the pH of Zn-Cr LDH is higher than the saturated pH of CO_2. A higher the reaction rate for the reduction of H^+ to H_2 leads to a greater increase in pH. Thus, Zn-CrLDH8 exhibits a superior photocatalytic activity for water splitting than Zn-CrLDH4, as reflected in the higher pH increase observed in Zn-CrLDH8. Moreover, Zn-CrLDH8 maintains its stability at higher reaction temperatures, as shown in Figure 5 by the consistent pH of the solution at 100 °C and at room temperature.

3.2.2 Effect of Cu or Cu_2O substitution on Zn-Cr LDH on photocatalyst performance

Zn-Cr LDH is primarily active in water splitting reactions and exhibits limited capacity on reducing CO_2 to formic acid. It is hyphotesized that the insufficient electron photoexcitation ability of Zn-CrLDH for CO_2 reduction to formic acid is due to the less negative position of its conduction band and competition between H^+ reduction (-0.41 V vs SHE) and CO_2 reduction to CO (-0.52 V vs SHE), which has a more positive reduction energy level than that required for the reduction of CO_2 to formic acid (-0.61 V vs SHE). It is also suspected that the lack of activity of Zn-Cr LDH in the formic acid reduction reaction is also due to reliance on a single photosystem. UV-Vis diffuse reflectance spectroscopy reveals that Zn-CrLDH absorps light primarily in the range of 345-485 nm. Formic acid production requires light with a wavelength below 543 nm for one photosystem and below 804 nm for two photosystems [15]. Therefore, an additional photosystem is needed to complement the light absorbed by Zn-CrLDH. In this study, Cu and Cu_2O were proposed as complementary materials. UV-Vis diffuse reflectance spectra showed an absorption region at a wavelength beyond 675 nm, indicating the presence of two photosystems of Zn-Cr LDH with Cu or Cu_2O.

The photocatalyst activity test using 0.3Cu_2O@Zn-CrLDH and 0.3Cu@Zn-CrLDH was conducted at the room temperature. The pH of the reaction solution is shown in Figure 5. Only the reaction solution using 0.3Cu_2O@Zn-CrLDH exhibited a pH below the saturated CO_2 pH, indicating the presence of formic acid. The reaction temperature was then increased to 60 °C and 100 °C to accelerate the reaction rate. However, the pH profile of 0.3Cu_2O@Zn-CrLDH showed a decrease in photocatalyst activity in these higher temperatures. In contrast, the pH profile of the 0.3Cu@Zn-Cr LDH showed an increase in photocatalyst activity with rising the reaction temperature, indicating improved performance at elevated temperatures.

The solution resulting from the reaction which was suspected to contain formic acid, was analyzed qualitatively and quantitatively by Gas Chromatography Mass Spectrometry (GC-MS). A calibration curve was constructed from the chromatogram of a 0.01 M formic acid standard solution, plotting chromatogram vs. the concentration in Molar units. This allowed the determination of formic acid concentration in each resulting solution, as presented in Table 1. The calculated formic acid per gram of photocatalyst corresponds to the pH profile shown in Figure 5. The highest yield of formic acid, 21.62 $\mu mol.g_{cat}^{-1}.h^{-1}$, was obtained at a reaction

Table 1. The amount of formic acid per gram of photocatalyst formed

No	Photocatalyst	Reaction Temperature (°C)	Solution pH	Obtained HCOOH ($\mu mol.g_{catalyst}^{-1}.h^{-1}$)
1	0.3Cu@Zn-CrLDH	60	6.81	0.64
2	0.3Cu@Zn-CrLDH	100	6.63	21.62
3	0.3Cu_2O@Zn-CrLDH	25	6.82	0.63

temperature of 100 °C in the presence of 0.3Cu@Zn-Cr LDH.

The photocatalytic activity of Cu_2O was demonstrated by producing 0.63 µmol.g_{cat}^{-1}.h^{-1} of formic acid at room temperature in the presence of 0.3Cu_2O@Zn-CrLDH photocatalyst. However, activity declined at higher reaction temperatures of 60 °C and 100 °C. This decline was attributed to the oxidation reaction of Cu_2O to CuO which deactivated the photocatalyst. CuO, being the most stable copper oxide, limits the photocatalytic activity. The self-oxidation of Cu_2O to CuO was confirmed in a study conducted by Toe *et al*. on Cu_2O oxidation during water splitting [24]. The reduction in Cu_2O activity is associated with the accumulation of holes (h^+) from photoexcited electrons. Since Cu_2O has a valence band energy higher (more negative) than the oxidation energy level of O_2/H_2O (+1.23 V vs SHE), it oxidizes itself to CuO [22]. This self-oxidation can be mitigated by adding h^+ scavengers (e.g. Na_2SO_3), facilitating the photoexcitation process to continue [24].

For the 0.3Cu@Zn-CrLDH, Cu self-oxidation produces Cu_2O, which retains photocatalytic activity. Zheng *et al*. investigated the oxidation mechanism of Cu-based oxygen carriers (Cu → Cu_2O → CuO) in chemical looping combustion [25]. Their findings indicated that the energy barrier for diffusion within the bulk phase of Cu (111) is lower than that in the Cu_2O bulk phase (111), favoring Cu_2O formation before eventual oxidation to CuO [25]. Consequently, the effect of reaction temperature on the 0.3Cu_2O@Zn-CrLDH and 0.3Cu@Zn-CrLDH photocatalysts differs due to this oxidation mechanism.

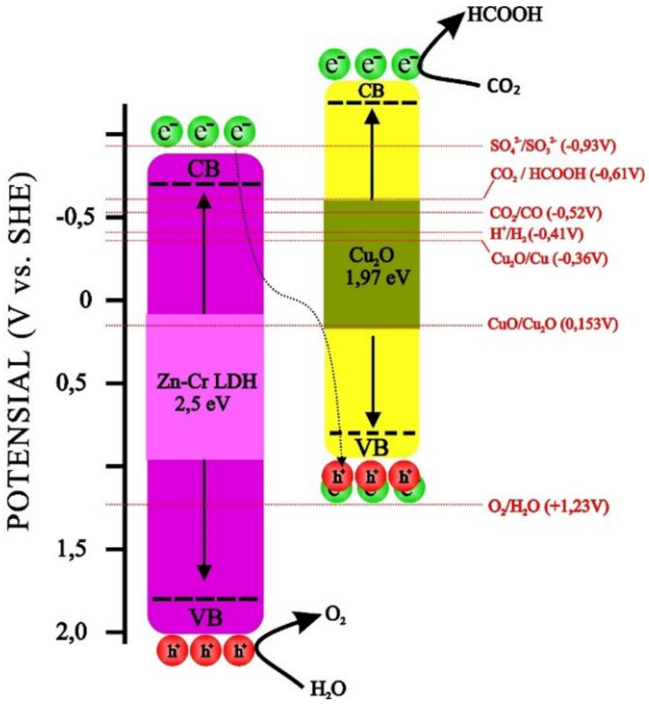

Figure 6. Z-scheme for the mechanism of CO_2 photoreduction to formic acid on Cu_2O@Zn-Cr LDH photocatalyst

3.2.3 Proposed photocatalytic mechanism

Natural photosynthesis occurs in two main stages within the functional units of photosystems, called Photosystems I (PSI) and Photosystems II (PSII), located in the thylakoid membranes of chloroplasts, which harvest photons of 700 and 680 nm, respectively [26]. These systems spatially separate oxygen evolution which occurs in PSII and CO_2 fixation in PSI [27]. This natural two-step process inspired the Z-scheme system design for artificial photosynthesis [28].

In the Z-scheme system, both Cu_2O and Zn-CrLDH act as photocatalysts that absorb visible light to generate electrons (e^-) in their conduction bands and holes (h^+) in the valence bands. Photoexcitation of electrons in Zn-CrLDH in PSI produces h^+ in the valence band O-2p (+1.83 V vs SHE). This energy level is sufficiently positive to oxidize water to oxygen, which happens at +1.23 V vs SHE. Simultaneously, electrons generated in the Cr-3dt_{2g} conduction band (-0.69 V vs SHE) transfer to the Cu_2O valence band (+0.84 V vs SHE), facilitating electron flow between systems.

In photoexcitation of Cu_2O in PSII, h^+ is neutralized by e^- from the Cr-3dt_{2g} conduction band so that the electron recombination process in Cu_2O can be suppressed. The conduction band of photoexcited Cu_2O (-1.13 V vs SHE) has a more negative energy level than the CO_2/HCOOH reduction potential (-0.61 V vs SHE), facilitating the reduction reaction of CO_2 to formic acid in the Cu_2O conduction band. The Z-scheme for the mechanism of CO_2 photoreduction to formic acid on Cu_2O@Zn-Cr LDH photocatalyst is illustrated in Figure 6. The data regarding the energy levels of the valence band and conduction band as well as for reduction level for each compound shown in Figure 6 refer to the research results Wang *et al*. [29].

However, self-oxidation of Cu_2O to CuO, triggered by h^+ accumulation deactivates PSII. When PSII is deactivated, electrons (e^-) in the Cr-3dt_{2g} conduction band cannot transfer to Cu_2O. Instead, these electrons in PSI reduce H^+ in the solution to form H_2 at a reduction potential of -0.41 V vs. SHE. This alternative pathway reduces the availability of H^+ in the solution, leading to an increase of pH when using 0.3C_2O@Zn-CrLDH at a reaction temperature of 60 °C and 100 °C. In contrast, for 0.3Cu@Zn-CrLDH, self-oxidation of Cu to Cu_2O occurs instead at a reaction temperatures of 60 °C and 100 °C. This allows electrons from PSI to transfer to PSII, where these electrons participate in the reduction of CO_2 to formic acid. This reaction does not significantly consume H^+ but instead fixes CO_2 into reduced carbon species, maintaining a lower pH when using 0.3Cu@Zn-CrLDH at 60 °C and 100 °C compared to CO_2-saturated solutions.

The effects of reduced crystallinity and structural changes in hydrotalcite which have previously been discussed did not significantly affect the photocatalytic activity of 0.3Cu_2O@Zn-CrLDH and 0.3Cu@Zn-Cr LDH. It was proven that all prepared photocatalyst effectively produced formic acid. From Figure 4, it can be seen that the Zn-CrLDH8, Zn-CrLDH4, 0.3Cu_2O@Zn-CrLDH and 0.3Cu@Zn-CrLDH have the similar absorption spectra for UV and visible light up to 655 nm. It is proven that all the photocatalysts prepared have the same CrO_6 octahedral structure because they have the same absorption sites on the LMCT, MMCT and d-d transitions on Cr^{3+} $^4A_{2g} \rightarrow {}^4T_{1g}$ (F) and $^4A_{2g} \rightarrow {}^4T_{2g}$ (F) ions. This results is in agreement with Parida and Mohapatra which stated that photoexcitation of the octahedral CrO_6 structure is the most crucial process in carrying out the water splitting reaction [14]. In addition, Cu_2O emerged as the most crucial site for photoreduction of CO_2 to formic acid, as its conduction band has a more negative potential than the CO_2/HCOOH reduction potential.

4. Conclusions

Based on the results of this study it can be concluded reducing the coprecipitation pH during Zn-Cr LDH preparation decreases the peaks associated with the zincite phase. From the UV-Vis diffuse reflectance spectroscopy spectrum, the 0.3Cu_2O@Zn-CrLDH and 0.3Cu@Zn-CrLDH demonstrated a better performance under the visible light compared to Zn-CrLDH8 and Zn-CrLDH4, with an absorption region at a wavelength of more than 675 nm. The highest yield of formic acid was achieved at 21.62 $\mu mol.g_{cat}^{-1}.h^{-1}$ at a reaction temperature of 100 ^oC using a 0.3Cu@Zn-Cr LDH. Differences in formic acid recovery between 0.3Cu_2O@Zn-CrLDH and 0.3Cu@Zn-CrLDH are attributed to the self-oxidation mechanism of Cu and/or Cu_2O due to the accumulation of holes (h^+) in their valence band.

Credit Author Statement

Author Contributions: *J. Rizkiana*: (Conceptualization, Methodology, Investigation, Resources, Data Curation, Writing, Review and Editing, Supervision); *D. Auliardi*: (Investigation, Data Curation, Writing); *A. C. A. Zahra*: (Writing, Review and Editing); *F. Thadeo*: (Writing, Review and Editing); *W. H. Saputera*: (Data Curation, Review and Editing); *T. H. Soerawidjaja*: (Conceptualization, Methodology, Data Curation, Review and Editing, Supervision); *H. Devianto*: (Data Curation, Review and Editing, Supervision). All authors have read and agreed to the published version of the manuscript.

References

[1] Wennersten, R., Sun, Q., Li, H. (2015) The future potential for Carbon Capture and Storage in climate change mitigation – an overview from perspectives of technology, economy and risk, *J. Clean. Prod.* 103, 724–736. DOI: 10.1016/j.jclepro.2014.09.023.

[2] Zhang, X., Guo, S.X., Gandionco, K.A., Bond, A.M., Zhang, J. (2020) Electrocatalytic carbon dioxide reduction: from fundamental principles to catalyst design, *Mater. Today Adv.* 7, 100074. DOI: 10.1016/j.mtadv.2020.100074.

[3] Daiyan, R., Lu, X., Ng, Y.H., Amal, R. (2017) Liquid Hydrocarbon Production from CO2 : Recent Development in Metal-Based Electrocatalysis, *ChemSusChem*. 10, 4342–4358. DOI: 10.1002/cssc.201701631.

[4] Marpani, F., Pinelo, M., Meyer, A.S. (2017) Enzymatic conversion of CO2 to CH3OH via reverse dehydrogenase cascade biocatalysis: Quantitative comparison of efficiencies of immobilized enzyme systems, *Biochem. Eng. J.* 127, 217–228. DOI: 10.1016/j.bej.2017.08.011.

[5] Gao, J., Jia, C., Liu, B. (2017) Direct and selective hydrogenation of CO2 to ethylene and propene by bifunctional catalysts, *Catal. Sci. Technol.* 7, 5602–5607. DOI: 10.1039/c7cy01549F.

[6] Aresta, M., Dibenedetto, A., Angelini, A. (2013) The changing paradigm in CO2 utilization, *J. CO2 Util.* 3–4, 65–73. DOI: 10.1016/j.jcou.2013.08.001.

[7] Olah, G.A., Prakash, G.K.S., Goeppert, A. (2011) Anthropogenic chemical carbon cycle for a sustainable future, *J. Am. Chem. Soc.* 133, 12881–12898. DOI: 10.1021/ja202642y

[8] Enthaler, S., Von Langermann, J., Schmidt, T. (2010) Carbon dioxide and formic acid—the couple for environmental-friendly hydrogen storage?, *Energy Environ. Sci.* 3, 1207–1217. DOI: 10.1039/B907569K.

[9] Wang, W.H., Himeda, Y., Muckerman, J.T., Manbeck, G.F., Fujita, E. (2015) CO2 Hydrogenation to Formate and Methanol as an Alternative to Photo- and Electrochemical CO2 Reduction, *Chem. Rev.* 115, 12936–12973. DOI: 10.1021/acs.chemrev.5b00197

[10] Kondratenko, E.V., Mul, G., Baltrusaitis, J., Larrazábal, G.O., Pérez-Ramírez, J. (2013) Status and perspectives of CO2 conversion into fuels and chemicals by catalytic, photocatalytic and electrocatalytic processes, *Energy Environ. Sci.* 6, 3112–3135. DOI: 10.1039/C3EE41272E.

[11] Kianička, J., Čík, G., Šeršeň, F., Špánik, I., Sokolík, R., Filo, J. (2019) Photo-Reduction of CO_2 by VIS Light on Polythiophene-ZSM-5 Zeolite Hybrid Photo-Catalyst, *Molecules*. 24, DOI: 10.3390/molecules24050992.

[12] Lingampalli, S.R., Ayyub, M.M., Rao, C.N.R. (2017) Recent Progress in the Photocatalytic Reduction of Carbon Dioxide, *ACS Omega*. 2, 2740–2748. DOI: 10.1016/j.cattod.2017.10.006

[13] Yang, Z.-z., Wei, J.-j., Zeng, G.-m., Zhang, H.-q., Tan, X.-f., Ma, C., Li, X.-c., Li, Z.-h. (2019) Chang Zhang, A review on strategies to LDH-based materials to improve adsorption capacity and photoreduction efficiency for CO2, *Coord. Chem. Rev.* 386, 154–182. DOI: 10.1016/j.ccr.2019.01.018.

[14] Parida, K., Mohapatra, L. (2012) Recent progress in the development of carbonate-intercalated Zn/Cr LDH as a novel photocatalyst for hydrogen evolution aimed at the utilization of solar light, *Dalton Trans.* 41, 1173–1178. DOI: 10.1039/C1DT10957J.

[15] Bolton, J.R. (1978) Solar fuels: The production of energy-rich compounds by the photochemical conversion and storage of solar energy, *Science.* 202, 705–711. DOI: 10.1126/science.202.4369.705

[16] Shang, Y., Sun, D., Shao, Y., Zhang, D., Guo, L., Yang, S. (2012) A Facile Top-Down Etching To Create a Cu2O Jagged Polyhedron Covered with Numerous {110} Edges and {111} Corners with Enhanced Photocatalytic Activity, *Chem. – A Eur. J.* 18, 14261–14266. DOI: 10.1002/chem.201201882.

[17] Lu, M., Zhang, J., Yao, Y., Sun, J., Wang, Y., Lin, H. (2018) Renewable energy storage via efficient reversible hydrogenation of piperidine captured CO2, *Green Chem.* 20, 4292–4298. DOI: 10.1039/C8GC00954F.

[18] Bookin, A.S., Cherkashin, V.I., Drits, V.A. (1993) Reinterpretation of the X-Ray Diffraction Patterns of Stichtite and Reevesite, *Clays Clay Miner.* 41, 631–634. DOI: 10.1346/CCMN.1993.0410514.

[19] Kloprogge, J.T., Hickey, L., Frost, R.L. (2005) The effect of varying synthesis conditions on zinc chromium hydrotalcite: a spectroscopic study, *Mater. Chem. Phys.* 89, 99–109. DOI: 10.1016/j.matchemphys.2004.08.035.

[20] Rutt, O.J., Williams, G.R., Clarke, S.J. (2006) Reversible lithium insertion and copper extrusion in layered oxysulfides, *Chem. Commun.* 2869–2871. DOI: 10.1039/B605105G.

[21] Neuburger, M.C., von Cuprooxyd, P.d.G. (1931) Cu2O, *Zeitschrift Für Phys.* 67, 845–850. DOI: 10.1002/zaac.19311970119

[22] Jiang, H., Katsumata, K., Hong, J., Yamaguchi, A., Nakata, K., Terashima, C., Matsushita, N., Miyauchi, M., Fujishima, A. (2018) Photocatalytic reduction of CO2 on Cu2O-loaded Zn-Cr layered double hydroxides, *Appl. Catal. B Environ.* 224, 783–790. DOI: 10.1016/j.apcatb.2017.11.011.

[23] Ceulemans, A., Coninckx, B., Görller-Walrand, C., Jacobs, H., Bock, J. (1988) The ligand field spectrum of K3[Cr(OH)6], *Chem. Phys. Lett.* 150, 127–128. DOI: 10.1016/0009-2614(88)80408-1.

[24] Toe, C.Y., Zheng, Z., Wu, H., Scott, J., Amal, R., Ng, Y.H. (2018) Photocorrosion of Cuprous Oxide in Hydrogen Production: Rationalising Self-Oxidation or Self-Reduction, *Angew. Chemie Int. Ed.* 57, 13613–13617. DOI: 10.1002/anie.201807647.

[25] Zheng, C., Cao, J., Zhang, Y., Zhao, H. (2020) Insight into the Oxidation Mechanism of a Cu-Based Oxygen Carrier (Cu → Cu2O → CuO) in Chemical Looping Combustion, *Energy & Fuels.* 34, 8718–8725. DOI: 10.1021/acs.energyfuels.0C00941.

[26] Yahia, E.M., Carrillo-López, A., Barrera, G.M., Suzán-Azpiri, H., Bolaños, M.Q. (2019) Chapter 3. Photosynthesis, *Postharvest Physiol. Biochem. Fruits Veg.* 47–72. DOI: 10.1016/B978-0-12-813278-4.00003-8.

[27] Toporik, H., Dobson, Z., Mazor, Y. (2021) Photosynthesis | The Photosystem I Complex of Oxygenic Photosynthesis, *Encycl. Biol. Chem.* Third Ed. 2, 191–206. DOI: 10.1016/B978-0-12-819460-7.00253-X.

[28] Wu, J., Huang, Y., Ye, W., Li, Y. (2017) CO2 Reduction: From the Electrochemical to Photochemical Approach, *Adv. Sci.* 4, 1700194. DOI: 10.1002/ADVS.201700194.

[29] Wang, C., Ma, B., Xu, S., Li, D., He, S., Zhao, Y., Han, J., Wei, M., Evans, D.G., Duan, X. (2017) Visible-light-driven overall water splitting with a largely-enhanced efficiency over a Cu2O@ZnCr-layered double hydroxide photocatalyst, *Nano Energy*. 32, 463–469. DOI: 10.1016/j.nanoen.2017.01.010.